J. Micromech. Microeng. **17** (2007) 1052–1058 doi:10.1088/0960-1317/17/5/027

Optimized liquid DEP droplet dispensing

R Ahmed and T B Jones

Department of Electrical and Computer Engineering University of Rochester, Rochester, NY 14627-0167, USA

E-mail: jones@ece.rochester.edu

Received 13 February 2007, in final form 23 March 2007
Published 24 April 2007
Online at stacks.iop.org/JMM/17/1052

Abstract
Dielectrophoretic droplet dispensing on a substrate relies on initial actuation of the liquid to form a uniform, sessile rivulet along the length of coplanar electrodes, and subsequent capillary-driven instability to form the droplets after the voltage is removed. Periodic bumps disposed along the length of the structure promote droplet formation by establishing an initial, static perturbation from which the instability evolves. Droplet uniformity, essential for applications in the laboratory-on-a-chip, is promoted if the bumps are spaced close to the most unstable wavelength predicted by Rayleigh's cylindrical jet theory. Proper sizing of the bumps guarantees good coverage by the droplets without compromising reliable droplet formation. Finally, if one of the coplanar electrodes is divided into two electrically addressable sections, and then if the voltage application to the sections is sequenced to trap liquid along the active structure, precisely positioned droplet dispensing of very uniform volume results. The experiments reported in this paper demonstrate the effectiveness of these enhancements. To achieve further improvements, the analytical approaches taken in the present work will have to be supplemented or replaced by numerical simulations of the capillary-driven transient hydrodynamics.

(Some figures in this article are in colour only in the electronic version)

Introduction

The most promising microfluidic 'plumbing' systems proposed for application in the laboratory-on-a-chip (LOC) and, indeed, for the larger class of micro-total-analysis systems (microTAS), use electrical forces to pump, transport or manipulate the liquid phase. Principal advantages of electrical systems include geometric simplicity, ease of fabrication, absence of moving parts and voltage-based control. Microfluidic schemes exploiting electromechanical forces, such as electrowetting-on-dielectric (EWOD) or liquid dielectrophoresis (DEP), are now receiving considerable attention due to their simple, open geometries. EWOD and DEP have the particular attraction of being amenable to droplet-based microfluidics, where droplets, dispensed and then moved about, serve as basic units of transport and analysis. Droplets can contain particulate matter of interest, say cells, DNA or marker particles, or the droplets themselves can be reagents in a chemical microreactor or processor. In any case, EWOD and DEP microfluidic schemes are particularly amenable for dispensing droplets and then transporting, mixing and otherwise manipulating them on a chip.

EWOD schemes have been studied for some years, and a broad array of very interesting demonstrations of their possibilities in the laboratory on a chip has been reported [1–4]. Liquid DEP is the newcomer [5], featuring easy-to-fabricate, open geometries along with the capability to dispense and manipulate droplets down to tens of picoliters, that is, approaching ink-jet technology. In a recent work, we described the basics of droplet formation [6] and some issues critical to the dynamic performance of liquid DEP actuation [7]. In this paper, we report improvements achieved in the reliability and precision of droplet dispensing over the size range from ~10 pl to 100 nl.

Phenomenology

The basic geometry of the liquid DEP droplet dispenser, shown in figure 1, consists of two parallel and coplanar electrodes patterned on an insulating substrate and then coated with a dielectric layer to insulate them electrically and to passivate

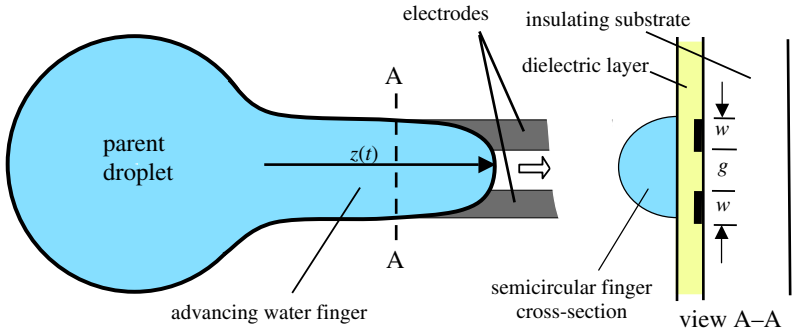

Figure 1. Basic geometry of the coplanar liquid DEP structure for droplet formation. When sufficient ac voltage is applied to the dielectrically coated electrodes, a finger protrudes from the parent droplet and moves along the structure at speeds >10 cm s^{-1}. The cross-section of the finger, shown in view A–A, is semicircular. The electrodes are coated with a dielectric layer for passivation and electrical insulation.

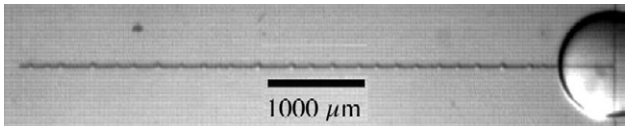

Figure 2. DI water droplets formed by capillary instability on a 6 mm long, coplanar electrode structure of dimensions $w = 10$ μm and $g = 15$ μm. There are 26 very irregularly spaced droplets having an average volume of 37 pl. Dielectric coating is 1.5 μm of Teflon AF-2400^{TM} with a top coat of Shipley 1805^{TM} photoresist.

them against electrolysis. A thin hydrophobic treatment is applied on top of the dielectric layer. Refer to the appendix for a summary of fabrication details. In operation, a microliter-sized droplet of DI water or some aqueous medium is manually dispensed atop one end of the electrodes. When ac voltage at ~50 to 100 kHz is applied, a rivulet or liquid finger protrudes from the sessile droplet and travels rapidly along the electrodes to the other end. The finger assumes a nearly semi-circular cross-sectional shape, as shown in view A–A of figure 1, that is almost uniform along its length $z(t)$ as it extends. As long as the electrode width w and space between the electrodes, g, are approximately equal, the finger usually covers the entire structure, that is, from the outer edge of one electrode to the outer edge of the other. When the finger reaches the end of the structure, motion stops and the stationary liquid settles into a hydrostatic equilibrium established primarily by the non-uniform electric field[1].

The rivulet, semicircular and uniform in cross-section along its length, remains stable until voltage is removed, at which time the familiar capillary jet hydrodynamic instability ensues. The instability breaks up the liquid into droplets spaced rather uniformly along the co-planar electrode structure[2]. Figure 2 shows a structure with 26 droplets that have formed along an electrode structure of cross-sectional dimensions $w = 10$ μm and $g = 15$ μm, and length 6 mm. The average droplet volume calculated from measuring the diameters of all the sessile droplets is ~37 pl.

[1] The nonuniform electric field of the coplanar electrodes contains the liquid in a hydrostatic equilibrium analogous to a capillarity structure. Liquid dielectrophoresis is best not thought of as a pumping mechanism.

[2] The URL provided here has videos showing the dynamics of DEP actuation and droplet formation: www.ece.rochester.edu/users/jones/index.html.

Capillary instability

Droplets form because when the non-uniform electric field is removed its stabilizing influence is lost and capillarity becomes dominant. The resulting hydrodynamic instability is familiar as the well-known phenomenon exhibited by cylindrical liquid jets, and exploited in ink-jet printers, flow cytometers and liquid spraying apparatus. Rayleigh was the first to model the inviscid, surface dynamics of the free, cylindrical jet [8]. He found that disturbances at all wavelengths longer than $\lambda_c = 2\pi R$ are unstable, and further that harmonic disturbances at wavelength $\lambda^* = 9.016R$ grow fastest, where R is the radius of the unperturbed jet.

Davis investigated the behavior of rivulets resting on a flat surface by developing a linearized model for the surface hydrodynamics [9]. He showed that the only significant factor differentiating the behavior of the sessile rivulet from the surface dynamics of the free cylindrical jet is the influence of the constraint at the liquid/solid contact line. Schiaffino and Sonin extended the model of Davis, deriving a predictive equation for the most unstable wavelength [10]. Interestingly enough, their work revealed that, in most cases, the difference between the sessile rivulet and Rayleigh's cylindrical jet is quite small. For application in liquid DEP droplet dispensing, the difference is smaller than the measurement uncertainty, meaning that Rayleigh's original expression for λ^* adequately predicts the unstable dynamics of rivulets. This conclusion is borne out in our results if we assume for modeling purposes that (i) the initial contact angle $\theta_c = 90^\circ$ and (ii) the contact line is fixed along the outer edges of the electrodes. An initial contact angle of $\theta_c = 90^\circ$ conforms well to our observations and, so long as the voltage is on, matches the requirement that the tangential electric field be continuous at all points on the curved periphery of the liquid/air boundary. A video frame from typical experiment is shown in figure 2.

Droplet formation results

We tested Rayleigh's theory against experimental data obtained from the coplanar structure, assuming $R = w + g/2$ for the radius of the semicircular cross-section of the rivulet, as suggested in figure 1:

$$(\lambda^*)_{calc} = 9.016R = 9.016(w + g/2). \quad (1)$$

Table 1. Droplet dispensing data for four coplanar DEP structures. Liquid retention is a measure of the total volume of all droplets, expressed as a percentage of the total inventory of the rivulet before the voltage is removed. Bumps have little effect on the net retention of liquid. Rather, the electrode structure width and liquid viscosity are the most significant factors, presumably because viscous drag, more significant for narrower structures, retards the liquid from being pulled back.

Electrode dimensions: $w/g/w$	Finger diameter: $(2w+g)$ (μm)	Average droplet volume: V_{drop}	Liquid retention (%)	Bump spacing: s	Average measured droplet spacing: $\langle s\rangle_{drop}$	Most unstable wavelength $(\lambda^*)_{calc}$: (μm)
50/50/50	150	~60 nl	~26	No bumps	Very irregular spacing	680
20/20/20	60	~200 pl	~33	No bumps	Very irregular spacing	270
10/20/10	40	~100 pl	~82	200 μm	~200 μm	180
5/10/5	20	~10 pl	~84	100 μm	~100 μm	90

In an experiment performed with a 6 mm long and very narrow structure, $w = 10$ μm and $g = 15$ μm, the calculated, most unstable wavelength, $(\lambda^*)_{calc} = 158$ μm, correlated well to the average measured drop-to-drop spacing, $\langle s\rangle_{drop} = 160$ (± 54) μm. The large standard deviation, ± 54 μm, is probably attributable to variations in the surface wetting conditions along the length of the open structure.

Closely related to the issue of spacing is the droplet volume. If all liquid in the initial rivulet inventory goes into the droplets, then the volume per droplet should be

$$V_{drop} = \pi R^2 \lambda^*/2. \qquad (2)$$

However, it is found that not all the liquid inventory ends up in the droplets. Instead, when voltage is removed, a competition arises between the hydrodynamic instability, seeking to pinch off and form droplets, and the surface tension force, seeking to pull liquid back into the parent droplet. This competition is clearly evident in one of the videos available at our research website (see footnote 2). For the experiment shown in figure 2, the total volume of liquid retained within the droplets is ~80% of the initial rivulet inventory, $\pi R^2 L/2$, where L is the rivulet length. The data in table 1 reveal that liquid retention is strongly dependent on the overall width of the electrodes, presumably due to the influence of viscous friction. The percent volume retained increases from ~26% up to 84% as the structure width is reduced from 150 to 20 μm.

Assessment

Table 1 indicates that the most unstable wavelength λ^* derived from Rayleigh's hydrodynamic model for a cylindrical liquid jet provides a fair prediction of the spacing and average volume for droplets formed in the liquid DEP dispenser. This is true over the three-order-of-magnitude range of droplet volumes one obtains by changing the electrode structure width, that is, $2w + g$, over one order of magnitude. On the other hand, the experimentally realized droplet spacings are highly irregular and their volumes are non-uniform. Furthermore, the total amount of liquid retained in the droplets from the original rivulet volume is very unpredictable. Such imprecision translates to unacceptably poor performance for applications in the laboratory-on-a-chip. The following sections of this paper describe certain enhancements to the electrode design that largely resolve these problems.

Spacing of bumps

To improve the uniformity of droplet spacing and volume, semicircular 'bumps' are patterned into the coplanar electrodes. Figure 3(*a*) shows the basic DEP structure modified by periodic bumps on the outside edges of the coplanar electrodes. Though their use was successfully demonstrated very early [5], the importance of the bump spacing for precision droplet dispensing was not immediately recognized. Originally, it was believed that the bumps function merely as collection regions where the droplets form preferentially because the field gradient at the curved edges of the bumps tends to attract liquid while the electric field is turned on. But we show here that the actual mechanism is more complex. Surface tension dominates after voltage is removed. The bumps' principal function, then, is to impose the static, spatially harmonic, initial condition upon the semicircular rivulet that determines the course of the instability once the stabilizing influence of the non-uniform electric field is removed. It is for this reason that the spacing of the bumps is crucial to precision droplet dispensing. The mechanism is depicted in figure 3(*b*).

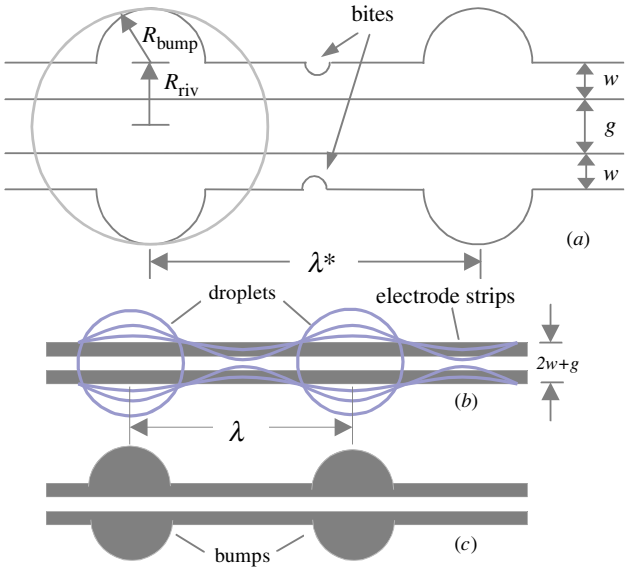

Figure 3. Bump structures establish initial conditions, thus regulating the Rayleigh instability that leads to droplet formation. (*a*) Definitions of droplet-forming bump quantities. As in figure 1, we assume that the radius of the static rivulet prior to droplet formation is $w + g/2$, the bumps are optimally spaced, i.e., $s = \lambda^*$, and the dispensed droplets have radii $R_{drop} = R_{riv} + R_{bump}$. The bites, intended to help pinch off the rivulet into droplets, were found ineffective. (*b*) Evolution of the capillary instability. (*c*) Corresponding placement of bumps to establish initial condition for dominance of the most unstable wavelength.

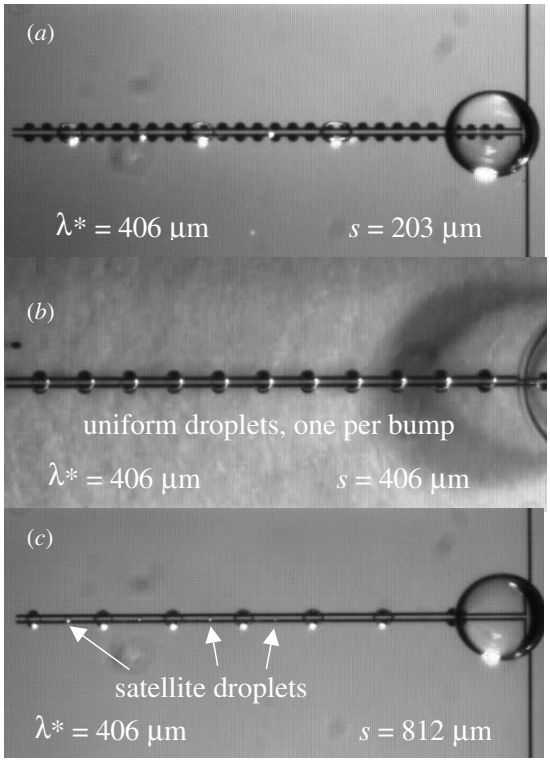

Figure 4. Experimental test of the effect of bump spacing on a similar electrode structure: $w = g = 30\ \mu$m. (*a*) Bump spacing $s = \lambda^*/2$, droplets do not form at each bump site. (*b*). Bump spacing $s = \lambda^*$, precise formation of 11 droplets on 11 uncovered bump sites. NB: the parent droplet overlapped the first bump site. (*c*). Bump spacing $s = 2\lambda^*$, irregular droplets and formation of small satellites midway between bumps.

To investigate the sensitivity of droplet formation to the bump spacing, a set of three similar test structures was designed and fabricated. The electrode width and gap for all three were fixed at $w = 30\ \mu$m and $g = 30\ \mu$m, but the spacing of the bumps, s, was varied from one-half to twice the ideal value: $(\lambda^*)_{\text{calc}} = 406\ \mu$m. The video frames in figures 4(*a*)–(*c*) reveal the results. In figure 4(*a*), the bumps are too close together, namely $s = (\lambda^*)_{\text{calc}}/2$, and as a result droplet formation is irregular; many of the bumps contain no droplets at all and the volumes are highly non-uniform. In figure 4(*c*), where the bumps are too far apart, namely $s = 2(\lambda^*)_{\text{calc}}$, a droplet forms at each bump but very small satellite droplets are observed midway between them. The droplet volumes again appear to be very non-uniform. For figure 4(*b*), showing the structure with the correct spacing $s = (\lambda^*)_{\text{calc}}$, uniform droplets form precisely at each uncovered bump site. Similar good performance is observed for structure widths down to ∼45 μm. Bumps spaced 30% greater than the most unstable wavelength, that is, $s = 1.3(\lambda^*)_{\text{calc}}$, produce irregular droplets.

Viscosity does have an effect on the fastest growing wavelength, as shown by Weber's equation [11]:

$$(\lambda^*)_{\text{We}} = 2\pi R\sqrt{2 + 6(Oh/2)^{0.5}} \qquad (3)$$

where $Oh = \rho\upsilon^2/\gamma R$ is the dimensionless Ohnesorge number, and υ, ρ and γ are kinematic viscosity, liquid density and surface tension, respectively. For dispensing water droplets in typically sized structures, the influence of viscosity may be neglected, but for ethylene glycol, with viscosity $\upsilon =$ 16 cP, the most unstable wavelength is increased by ∼30% [6], a result quantitatively confirmed by experiment.

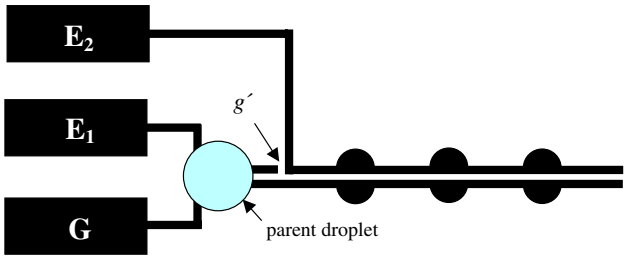

Figure 5. Droplet dispensing structure with a trapping feature. Initially, when both E_1 and E_2 are energized, a finger forms, jumps the gap g', moves along E_2. After the finger reaches the end at the right and stops, voltage to E_1 can be cut off. Shortly afterward, when the trapped liquid has had time to distribute itself uniformly, the voltage to E_2 is removed, allowing uniform droplets to form at the bumps.

We expended some effort to determine if small indentations, depicted in figure 3(*a*) and called 'bites', would promote the capillary instability leading to pinch off of drops. By themselves, bites do not seem to affect droplet formation. Furthermore, combining them with bumps, as depicted in figure 3(*a*), leads to two problems. If the bites are of a size large enough to constrict the capacitive current flow, localized Joule heating of the electrodes occurs. There is also evidence that the sharp edges of the bites promote electrical breakdown of the dielectric layer.

Control of liquid inventory

The data in table 1 reveal the strong tendency of surface tension to pull liquid back into the parent droplet when the voltage is removed. Even with the smaller structures, more than 15% of the initial inventory of the static rivulet is lost from droplet formation by this mechanism. The presence of bumps does not alleviate the problem. The result is an unacceptable level of uncertainty for individual droplet volumes. An effective solution to this problem is to trap the liquid along the bump structures using the three-electrode structure shown in figure 5. In this configuration, one of the electrode strips is divided into two separate sections, E_1 and E_2, and the voltages to these electrodes are independently controlled by electronic timer circuitry. The other electrode G is connected to ground. A typical operational sequence of the structure is described below. First, ac voltage is applied to both E_1 and E_2 to initiate finger formation and movement from left to right. The finger moves along E_1, jumping the gap g' and proceeding along E_2 until, at some time t_o, it reaches the end of the structure at the far right and fills up the structure. At time t_1, the voltage to E_1 is shut off, trapping virtually all the liquid in the static rivulet along the length of E_2. After an interval sufficient to equalize the distribution of liquid along the length of E_2, the voltage is removed from E_2 at time t_2.

Note that, at least for the simple operational mode described here, the timer controlling the voltage to E_1 must be set so that the finger completely fills E_2 with liquid, that is, $t_1 > t_o$. The transit time t_o can be determined from either

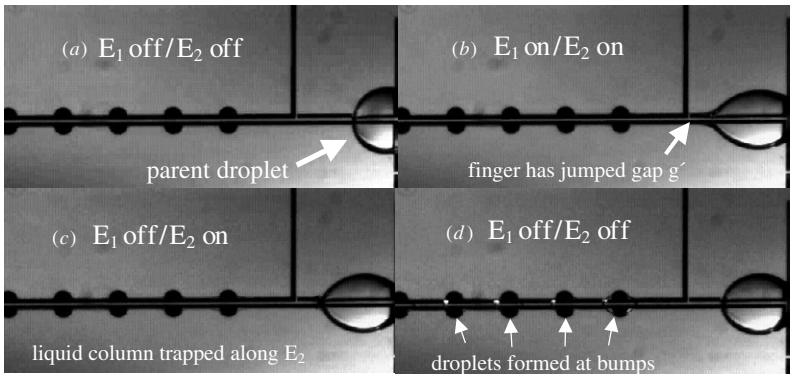

Figure 6. Sequence of video frames showing operation of the trapping structure: $w = 90\ \mu$m; $g = 60\ \mu$m; $g' = 40\ \mu$m. (*a*) No voltage applied, parent droplet atop the electrode structure before start of timed voltage sequence; (*b*) voltage applied to E_1 and E_2, liquid finger has jumped gap g' and liquid is filling the bumps; (*c*) E_1 is turned off, liquid rivulet is trapped along E_2; (*d*) E_2 is turned off, six droplets formed on six bump sites (only five bumps are visible).

empirical data or a dynamic model [7]. A better alternative now under investigation is to replace the timing circuitry with a feedback system including sensors to detect finger location and algorithm-based control of the voltages supplied to the electrodes [12]. The interval $t_2 - t_1$ need not be long, because capillary and DEP rapidly dispose of any non-uniformity in the distribution along E_2 once the liquid is trapped.

For satisfactory operation, the finger must reliably jump the gap g' when the voltage is turned on. At the same time, surface flashover must be avoided. From experiment, we found that the most reliable performance is achieved for $g'/g \sim 0.7$. To get the finger to jump the gap for larger spacings, say $g'/g \sim 1$, the voltage must be increased so much that breakdown becomes common. Smaller values also inherently increase the risk of flashover. Some effort has been made to test other gap geometries, such as angular cuts, but we have reached no conclusion about their relative effectiveness.

The selected video frames in figure 6 provide a demonstration of a three-electrode structure. Upon application of voltage (∼200 V-rms at 100 kHz), a liquid finger forms and subsequently starts to move from right to left. The finger jumps the gap g' and continues to move forward. As it does, liquid is drawn from the parent droplet and the bumps start to fill. Once the liquid finger reaches the end of the structure, E_1 is shorted, trapping a semi-cylindrical water rivulet along the entire length of E_2. Then, E_2 is shorted, allowing the hydrodynamic instability to form the droplets, one at each of the six bump sites. Note that the field of view in these frames shows only five of the droplets that actually formed. Examination of the photomicrographs reveals that, within the error of measurement, at least 99% of the liquid is trapped and retained along E_2 and in the droplets. These droplets have good uniformity and are precisely centered over the bumps. We observed this same 99% retention for four structure widths, ranging from 60 to 240 μm and corresponding to droplet volumes from 400 pl to 26 nl.

A problem encountered with the three-electrode structure and evident from close examination of figure 6(*d*) is that sometimes the droplet formed at the bump site closest to the 'T' junction contains more liquid than the rest of the droplets further away. Another related manifestation of the problem is that sometimes, as shown in figure 7, small droplets form right

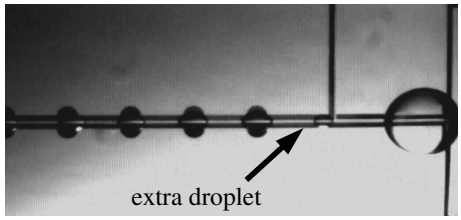

Figure 7. Formation of an unwanted droplet at the 'T' junction of the three-electrode structure, probably because the first bump is too far from the junction.

at the junction. To overcome this shortcoming of the droplet dispenser, a comprehensive optimization of the three-electrode geometry will be needed, including (i) proper placement of the first bump adjacent to the T, (ii) proper placement of the gap g' on the opposite side of the junction and (iii) determination of the optimum width of the trace connecting E_2 to its connection pad.

Bump size optimization

We envision applications in some lab-on-a-chip applications of DEP droplet dispensing where the bumps serve as integral elements of chemical/biochemical probes or sensor systems, in which case it might be important for each bump to be completely covered by liquid once the hydrodynamic instability has run its course. As long as the bumps are large enough to perform the function of initiating the Rayleigh instability, then it should be possible independently to optimize their size to promote complete coverage by the droplets with no waste. Accordingly, we performed an optimization of the bump radius R_{bump}, as defined in figure 3(*a*), to match the profiles of the bumps with the footprint of the sessile droplets. An assumption key to the analysis is that the bumps are spaced at $s = \lambda^*$. The volume of the droplet that forms at each bump is equal to the amount of liquid contained along length s of the static rivulet plus the increment contained in the bump, that is,

$$\frac{2\pi}{3}(R_{\mathrm{bump}} + R_{\mathrm{riv}})^3 \approx \frac{\pi}{2} R_{\mathrm{riv}}^2 \lambda^* + \frac{2\pi}{3} R_{\mathrm{bump}}^3. \qquad (4)$$

Substituting in for λ^* using equation (1) results in a quadratic equation which may be solved for R_{bump} in terms of R_{riv}. The

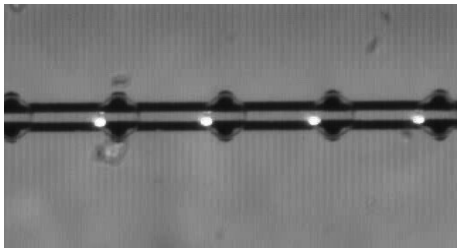

Figure 8. Water droplets of volume ∼400 nl formed on bumps of optimized size, $R_{bump} = R_{riv}$ with spacing $s = \lambda^*$. From observation, $R_{drop} \sim R_{riv} + R_{bump}$. Shifting the center of the bump radii to the midpoint of the electrodes and readjusting R_{bump} can eliminate the overlap noted in the corners. For this electrode structure, $w = 30\ \mu$m and $g = 30\ \mu$m.

physically meaningful root of equation (6) is $R_{bump} = 0.98R_{riv}$. This result was tested with a set of electrode structures with identical w and g values and the bump spacing s, but varied bump radii: $R_{bump}/R_{riv} = 0.67$, 1.0, 1.75 and 2.0. The smallest bump radius, $R_{bump} = 0.67R_{riv}$, yielded irregular droplet formation, presumably because the bumps were too small to initiate the instability reliably. All larger bump sizes produced regular, uniform droplets, but the structure with $R_{bump} = R_{riv}$ shown in figure 8 worked best in the sense that, as expected from the criterion imposed by equation (4), the droplet provided the best coverage of the bump with minimal overlap or uncovered bump area .

For the structures tested, the semicircular bumps are centered at the outer edges of the electrodes, as illustrated in figure 3(*a*), but this configuration is still not really optimal if the goal is for the drops to cover the bump area exactly with no overlap. The structure pattern should be redesigned by relocating the centers of the bumps to the centerline of the electrodes to achieve the best match of bump shape to droplet footprint. Future effort is needed to test such bump designs.

Discussion and conclusion

This paper reports improved droplet dispensing precision achieved by optimization of the electrode structures on open substrates using liquid dielectrophoretic actuation. The single most important design feature for the electrodes is to space the bumps at Rayleigh's most unstable wavelength defined by equation (1), that is, $s = \lambda^*$. Small indentations or 'bites' patterned midway between the bumps and intended to help precipitate the pinch-off of uniform droplets seem not to be effective. Another very effective strategy is to prevent the capillary-driven withdrawal of liquid back into the parent droplet by trapping the liquid using the three-electrode structure illustrated in figure 5. Application of voltage to the electrodes must be sequenced properly; in the experiments presented, a timer circuit that turns off the ac voltage to the different electrodes at preset times performs this function. The third design improvement is to size the bumps properly so that they (i) serve the crucial function of initiating the hydrodynamic instability and also (ii) match the footprint of each droplet to the actual area of the bumps.

While the experimental results demonstrate significant improvements to the precision and reliability of DEP droplet dispensing, they also point the way to further enhancements. For example, it should be possible to sense the advancing rivulet as it moves past fixed points along the structure and then to use these data in a feedback system to control the voltage magnitude and possibly the frequency. Closed-loop control promises to yield a far more robust and flexible scheme, very important considerations, given the high speed of liquid DEP actuation and the unavoidable variation of the wetting characteristics from one chip to another. A second enhancement would be to redesign the bumps so that they better conform to the actual outline of the sessile droplets formed on the surface.

In the present study, analytical approaches have been successfully employed to improve the performance of liquid DEP actuation and droplet dispensing; however, it must be recognized that numerical simulation will play a key role in further optimization efforts. One good example of the need for such a methodology is the problem of irregular droplet formation in the vicinity of the T junction of the three-electrode structure, as exemplified in figures 6(*d*) and 7. Optimization of this critical region of the electrodes requires detailed consideration of the capillary-driven, transient hydrodynamics. Another problem is the configuration of the gap g' in the three-electrode trap structure. As was recognized long ago in development of ink-jet printer technology, it might be useful to perform simulations of the evolution of the hydrodynamic instability that extend to its nonlinear stage. Furthermore, there are many other novel electrode structures worth testing that, while not amenable to analytical modeling, can be investigated via a combination of experiment and numerical simulation.

Acknowledgments

This work is based on the thesis of R Ahmed, submitted in partial fulfillment of the requirements for the PhD degree in Materials Science at the University of Rochester. The authors are grateful to V Derefinko for assistance with the electronic timer circuitry, and to C Bailey, K-L Wang and T Kanagasabapathi for helpful comments and other contributions. P Osborne built a test fixture used for some of the experiments. RA gratefully acknowledges internship support from NexPress Solutions, Inc., Rochester, NY. This work was supported in part by the National Science Foundation (USA), the Infotonics Technology Center (Canandaigua, NY, USA) and the Center for Future Health at the University of Rochester.

Appendix

The experiments upon which this paper was based were performed using electrode structures photolithographically patterned in 2–3 kÅ vapor-deposited Al upon borosilicate glass substrates. A variety of dielectric coatings were used, most typically SU-8 or Teflon AF 2400, in thicknesses ranging from 1.5 to 3 μm. Depending on experimental requirements, any of several different hydrophobic top coats, also spin-coated, were employed to achieve the optimum contact angle, including 1.5 μm Shipley 1805^{TM} negative photoresist and 0.5 μm

Teflon-AF^{TM}. Most experiments were conducted using deionized water, and an oil bath was often used to avoid heating and evaporation of the water.

References

[1] Seyrat E and Hayes R 2001 Amorphous fluoropolymers as insulators for reversible low-voltage electrowetting *J. Appl. Phys.* **90** 1383–6

[2] Prins M W J, Welters W J J and Weekamp J W 2001 Fluid control in multichannel structures by electrocapillary pressure *Science* **291** 277–80

[3] Welters W J J and Fokkink L G J 1998 Fast electrically switchable capillary effects *Langmuir* **14** 1535–8

[4] Pollack M G, Fair R B and Shenderov A D 2000 Electrowetting based actuation of liquid droplets for microfluidic applications *Appl. Phys. Lett.* **77** 1725–6

[5] Jones T B, Gunji M, Washizu M and Feldman M J 2001 Dielectrophoretic liquid actuation and nanodroplet formation *J. Appl. Phys.* **89** 1441–8

[6] Ahmed R and Jones T B 2006 Dispensing picoliter droplets on substrates using dielectrophoresis *J. Electrost.* **64** 543–9

[7] Wang K-L, Jones T B and Raisanen A 2007 Dynamic control of DEP actuation and droplet dispensing *J. Micromech. Microeng.* **17** 76–80

[8] Lord Rayleigh 1945 *The Theory of Sound* vol 2 (New York: Dover) p 359

[9] Davis S H 1980 Moving contact lines and rivulet instabilities: part 1. The static rivulet *J. Fluid Mech.* **98** 225–42

[10] Schiaffino S and Sonin A A 1997 Formation and stability of liquid and molten beads on a solid surface *J. Fluid Mech.* **343** 95–110

[11] Weber C 1931 Zum zerfall eines flüssigkeitsstrahles *Z. Angew. Math. Mech.* **11** 135–54

[12] Wang K-L 2006 Private communication, University of Rochester